TWMS J. App. and Eng. Math. V.15, N.7, 2025, pp. 1698-1714

NUMERICAL SOLUTION OF THE TIME-VARIABLE FRACTIONAL ORDER MOBILE-IMMOBILE ADVECTION-DISPERSION MODEL USING A HYBRID METHOD

S. FOADIAN[1*], R. POURGHOLI[1], §

Abstract. This paper introduces a hybrid numerical method combining the cubic B-spline collocation method with the implicit Euler approximation to solve the time-variable fractional order mobile-immobile advection-dispersion model (MIM-ADM). The model includes the Coimbra variable-order (VO) time fractional derivative, which is well-suited for dynamic system modeling. Cubic B-spline functions are employed for spatial discretization, offering both flexibility and efficiency in approximating solutions. The implicit Euler method accurately approximates the Coimbra VO time fractional derivative. Moreover, we establish that the proposed method achieves a convergence order of $\mathcal{O}(h_t^{2-\lambda(x,t)} + h_x^4)$. Numerical simulations confirm the accuracy of the method by comparing its results with analytical solutions. Evaluation metrics such as L_2 and L_∞ error norms demonstrate the method's efficacy in solving the MIM-ADM. This study highlights the effectiveness of the proposed approach in modeling and solving complex transport phenomena with high accuracy.

Keywords: Mobile-immobile advection-dispersion model, Cubic B-spline collocation method, Implicit Euler approximation, Numerical solution..

AMS Subject Classification: 65Nxx, 74G15.

1. Introduction

Fractional-order calculus has gained widespread attention in engineering and physical sciences over the past few decades for modeling diverse phenomena in robotic technology, bio-engineering, control theory, viscoelasticity, diffusion models, relaxation processes, and signal processing [2, 14]. This approach is particularly notable for its capability to describe complex systems, including anomalous diffusion and transport dynamics, which traditional integer-order models fail to capture accurately. Fractional-order derivatives, especially when variable in time or space, offer a comprehensive framework for these phenomena [6, 7, 13, 16, 18]. Recent advances in high-order numerical methods have significantly

[1] School of Mathematics and Computer Science, Damghan University, Damghan, Iran.
e-mail: s.foadian@std.du.ac.ir; https://orcid.org/0000-0001-7091-1254.
e-mail: pourgholi@du.ac.ir; https://orcid.org/0000-0003-4111-5130.
[*] Corresponding author.
§ Manuscript received: June 20, 2024; accepted: May 22, 2025.

This work is based upon research funded by Iran National Science Foundation (INSF) under project No. 4023391.

improved the accuracy of fractional partial differential equation solvers. For instance, a sixth-order spatial scheme was introduced for time-fractional diffusion equations, achieving high precision and computational efficiency [22]. The Coimbra variable-order fractional derivative has been recognized as a powerful tool in this context [3], as it allows the fractional order to vary dynamically, offering a more flexible modeling approach.

The MIM-ADM plays a crucial role in understanding transport processes in porous media, where substances transition between mobile and immobile phases. Traditional models often fail to accurately capture these processes, particularly when the fractional order varies over time. This limitation necessitates the development of advanced numerical methods. [10, 5]. Solving the time-variable fractional order MIM-ADM is essential for accurately modeling the complex behavior of solute transport in heterogeneous media, a key aspect of many scientific and engineering applications. In many natural and industrial processes, such as groundwater contamination, oil recovery, and pollutant transport in rivers, particle movement is not purely diffusive or advective but rather a combination of both, with intermittent periods of immobilization. Traditional advection-dispersion equations, which assume constant or integer-order derivatives, often fail to capture the heterogeneity and memory effects inherent in such systems. Fractional derivatives, particularly those of variable order, offer a more effective framework for describing these processes by accounting for both the memory effects and variability of transport dynamics. Furthermore, for variable-order fractional diffusion problems, optimal order finite difference and local discontinuous Galerkin methods have been proposed, providing robust and accurate solutions even when the fractional order varies in space and time [20].

In this paper, we study the time-variable fractional order MIM-ADM in the following form [21]:

$$\alpha_1 \frac{\partial \varphi(x,t)}{\partial t} + \alpha_2 D_t^{\lambda(x,t)} \varphi(x,t) = -\theta_1 \frac{\partial \varphi(x,t)}{\partial x} + \theta_2 \frac{\partial^2 \varphi(x,t)}{\partial x^2} + \mathcal{G}(x,t), \tag{1}$$

for $a < x < b$ and $0 < t < t_{\text{final}}$; with the initial and Dirichlet boundary conditions:

$$\varphi(x,0) = r_1(x), \qquad a \le x \le b, \tag{2}$$

$$\varphi(a,t) = r_2(t), \qquad \varphi(b,t) = r_3(t), \qquad 0 \le t \le t_{\text{final}}, \tag{3}$$

where $\alpha_1, \alpha_2 \ge 0$, $\theta_1, \theta_2 > 0$, $\mathcal{G}(x,t)$ represents the source term, and $r_1(x)$, $r_2(t)$, and $r_3(t)$ are known analytical functions. Also, $D_t^{\lambda(x,t)}$ is the Coimbra VO derivative operator, defined as follows [3]:

$$D_t^{\lambda(x,t)} \varphi(x,t) = \frac{1}{\Gamma(1-\lambda(x,t))} \int_0^t \frac{\partial \varphi(x,\tau)}{\partial \tau} (t-\tau)^{-\lambda(x,t)}\, d\tau,$$

where $0 < \lambda(x,t) < 1$ is a continuous function of two variables and $\Gamma(\cdot)$ is the Gamma function.

The main aim of this paper is to propose a hybrid numerical method based on the cubic B-spline collocation method and the implicit Euler approximation to obtain approximate solutions of (1)–(3). The theory of B-spline functions has attracted attention in the literature for the numerical solution of boundary value problems in science and engineering. The numerical solution of certain partial differential equations can be obtained using cubic B-spline functions. As examples, a cubic B-spline function was used to solve the generalized Burgers-Fisher and generalized Burgers-Huxley equations [12]. In [4], the cubic B-spline is used to solve the inverse parabolic system. The extended cubic B-spline functions was applied for the solution of the time-fractional Klein-Gordon equation [1]. A cubic B-spline basis functions was developed in [17] for the solution of time fractional

Burgers' equation involving Atangana-Baleanu derivative. The cubic B-Spline collocation method was used to solve the second order of the linear hyperbolic equation in [11]. In this work, a collocation method with cubic B-spline is used to discretize the time-variable fractional order MIM-ADM in the spatial direction, and the time fractional term is simulated by applying the implicit Euler approximation. The advantages of this method include:

(1) High spatial accuracy due to the flexibility of cubic B-splines in handling complex geometries and gradients,
(2) The implicit Euler method provides stability in time discretization, making the approach well-suited for solving complex time-dependent fractional differential equations.
(3) This hybrid method is particularly effective in modeling the complex transport dynamics in porous media with variable-order fractional derivatives, which traditional integer-order or constant-order models fail to capture accurately.

However, the disadvantages of the method include: High computational complexity, especially when dealing with large-scale problems, which may lead to longer computation times and dependence on precise initial conditions and model parameters, which may pose challenges in practical applications where such data is difficult to obtain.

The remainder of this paper is organized as follows: Section 2 details the cubic B-spline collocation method used for the numerical solution. Section 3 presents the description of the proposed method based on the cubic B-spline method and implicit Euler approximation. Numerical computations are discussed in Section 5, and concluding remarks are provided in Section 6.

2. Cubic B-spline functions

In this section, we describe the uniform cubic B-spline over the finite interval $[a, b]$. For this purpose, we divide the interval $[a, b]$ into M-subintervals by the set of $M + 1$ nodal points x_i, $0 \leq i \leq M$. This gives a partition $\pi : a = x_0 < x_1 < \cdots < x_{M-1} < x_M = b$ of $[a, b]$, where $\Delta x_i = x_i - x_{i-1}$, $\forall\ 1 \leq i \leq M$. The cubic B-splines are constructed for the partition

$$\Pi : x_{-2} < x_{-1} < x_0 = a < x_1 < \cdots < x_M = b < x_{M+1} < x_{M+2},$$

by using four fictitious nodes $x_{-2}, x_{-1}, x_{M+1}, x_{M+2}$.
If we assume that $\Delta x_i = h_x$, $\forall\ -1 \leq i \leq M + 2$, then the uniform cubic B-splines are defined by, [4],

$$B_i(x) = \frac{\Delta^4 F_x(x_{i-2})}{h_x^3},$$

where

$$F_x(x_i) = (x_i - x)_+^3 = \begin{cases} (x_i - x)^3, & x < x_i, \\ 0, & x \geq x_i, \end{cases}$$

and $\Delta^4 F_x(x_i)$ is the fourth forward difference with equally spaced nodes of third degree polynomial $F_x(x_i)$. After some simplification, we get

$$B_i(x) = \frac{1}{h_x^3} \begin{cases} (x - x_{i-2})^3, & x_{i-2} \leq x < x_{i-1}, \\ h_x^3 + 3h_x^2(x - x_{i-1}) + 3h_x(x - x_{i-1})^2 - 3(x - x_{i-1})^3, & x_{i-1} \leq x < x_i, \\ h_x^3 + 3h_x^2(x_{i+1} - x) + 3h_x(x_{i+1} - x)^2 - 3(x_{i+1} - x)^3, & x_i \leq x < x_{i+1}, \\ (x_{i+2} - x)^3, & x_{i+1} \leq x \leq x_{i+2}, \\ 0, & \text{otherwise}. \end{cases} \tag{4}$$

It can be easily see that the functions in $\{B_{-1}, B_0, \ldots, B_M, B_{M+1}\}$ are linearly independent on $[a, b]$, ([15]). By using splines defined in (4), the values of $B_i(x)$ and its derivatives at the nodes x_i's are given in Table 1.

TABLE 1. The values of $B_i(x)$ and its derivatives at the nodal points.

	$B_i(x)$	$B_i'(x)$	$B_i''(x)$
x_{i-2}	0	0	0
x_{i-1}	1	$3/h_x$	$6/h_x^2$
x_i	4	0	$-12/h_x^2$
x_{i+1}	1	$-3/h_x$	$6/h_x^2$
x_{i+2}	0	0	0

3. Description of the proposed method

In this section, we present the application of the cubic B-spline method and the implicit Euler approximation to obtain numerical solutions for the problem defined by equations (1)–(3).

3.1. **Space discretization by the cubic B-spline.** In this subsection, we introduce our method based on cubic B-spline functions for the discretization of spatial derivatives that appear in the MIM-ADM (1).
To apply the proposed method, we express $\varphi(x, t)$ using cubic B-spline functions. Let

$$\varphi^*(x, t_k) \cong \sum_{i=-1}^{M+1} \sigma_i^k B_i(x), \tag{5}$$

be the approximate solution of the problem (1) at the k-th time level, where σ_i^k is unknown time-dependent quantities to be determined.

Using approximate solution (5) and cubic B-spline (4), the approximate values at the knots of $\varphi^*(x_i, t_k)$ and its derivatives up to second order are determined in terms of the time parameters σ_i^k as

$$\varphi^*(x_i, t_k) = \sigma_{i-1}^k + 4\sigma_i^k + \sigma_{i+1}^k, \tag{6}$$

$$\varphi^{*\prime}(x_i, t_k) = \Big(\frac{3}{h_x}\Big)\Big(\sigma_{i+1}^k - \sigma_{i-1}^k\Big), \tag{7}$$

$$\varphi^{*\prime\prime}(x_i, t_k) = \Big(\frac{6}{h_x^2}\Big)\Big(\sigma_{i-1}^k - 2\sigma_i^k + \sigma_{i+1}^k\Big). \tag{8}$$

3.2. **Time discretization of the time fractional derivative.** In this subsection, our aim is to discretize the time-variable fractional order derivative. The VO derivative operator in equation (1) is discretized using the implicit Euler approximation as follows

[21]:

$$D_t^{\lambda_i^{k+1}}\varphi_i^{k+1} =\gamma^*\Big[\varphi(x_i,t_{k+1})-\varphi(x_i,t_k)\Big]+\gamma^*\sum_{j=1}^{k}\omega_{j,i}^{k+1}\Big[\varphi(x_i,t_{k-j+1})-\varphi(x_i,t_{k-j})\Big] +\mathcal{O}(h_t^{2-\lambda_i^{k+1}}), \tag{9}$$

where $\lambda_i^k=\lambda(x_i,t_k)$, and

$$\gamma^*=\frac{h_t^{-\lambda_i^{k+1}}}{\Gamma(2-\lambda_i^{k+1})}, \qquad \omega_{j,i}^{k+1}=(j+1)^{1-\lambda_i^{k+1}}-j^{1-\lambda_i^{k+1}},$$

where h_t is the time step. By omitting the small term $\mathcal{O}(h_t^{2-\lambda_i^{k+1}})$ in equation (9) and denoting φ^* as the approximation of φ, we obtain

$$D_t^{\lambda_i^{k+1}}(\varphi^*)_i^{k+1}=\gamma^*\Big[\varphi^*(x_i,t_{k+1})-\varphi^*(x_i,t_k)\Big]+\gamma^*\sum_{j=1}^{k}\omega_{j,i}^{k+1}\Big[\varphi^*(x_i,t_{k-j+1})-\varphi^*(x_i,t_{k-j})\Big]. \tag{10}$$

3.3. **Description of the numerical technique.** In equation (1), if we set the approximation (10) in this equation, we obtain

$$\begin{aligned}&\alpha_1\frac{\partial\varphi^*(x_i,t_{k+1})}{\partial t}+\alpha_2\gamma^*\varphi^*(x_i,t_{k+1})-\alpha_2\gamma^*\varphi^*(x_i,t_k)\\&+\alpha_2\gamma^*\sum_{j=1}^{k}\omega_{j,i}^{k+1}\Big[\varphi^*(x_i,t_{k-j+1})-\varphi^*(x_i,t_{k-j})\Big]=-\theta_1\frac{\partial\varphi^*(x_i,t_{k+1})}{\partial x}+\theta_2\frac{\partial^2\varphi^*(x_i,t_{k+1})}{\partial x^2}\\&\qquad+\mathcal{G}(x_i,t_{k+1}).\end{aligned} \tag{11}$$

With using the time derivatives is discretized in a forward finite difference fashion in equation (11), we have

$$\begin{aligned}\delta\varphi^*(x_i,t_{k+1})+\theta_1\frac{\partial\varphi^*(x_i,t_{k+1})}{\partial x}-\theta_2\frac{\partial^2\varphi^*(x_i,t_{k+1})}{\partial x^2}&=\mathcal{G}(x_i,t_{k+1})+\delta\varphi^*(x_i,t_k)\\&-\alpha_2\gamma^*\sum_{j=1}^{k}\omega_{j,i}^{k+1}\Big[\varphi^*(x_i,t_{k-j+1})-\varphi^*(x_i,t_{k-j})\Big],\end{aligned} \tag{12}$$

where $\delta=\frac{\alpha_1}{h_t}+\alpha_2\gamma^*$.

Now, substituting the approximate values (6)–(8) in equation (12) yield the following equation with the variable σ

$$\mu_1\sigma_{i-1}^{k+1}+\mu_2\sigma_i^{k+1}+\mu_3\sigma_{i+1}^{k+1}=\mathcal{A}(x_i,t_{k+1}), \tag{13}$$

where $i=0,1,\dots,M$, $k=0,1,\dots,$ and

$$\mu_1=\delta-\frac{3\theta_1}{h_x}-\frac{6\theta_2}{h_x^2}, \qquad \mu_2=4\delta+\frac{12\theta_2}{h_x^2}, \qquad \mu_3=\delta+\frac{3\theta_1}{h_x}-\frac{6\theta_2}{h_x^2},$$

also,

$$\begin{aligned}\mathcal{A}(x_i,t_{k+1})=&\mathcal{G}(x_i,t_{k+1})+\delta\Big[\sigma_{i-1}^k+4\sigma_i^k+\sigma_{i+1}^k\Big]\\&-\alpha_2\gamma^*\sum_{j=1}^{k}\omega_{j,i}^{k+1}\Big[(\sigma_{i-1}^{k-j+1}+4\sigma_i^{k-j+1}+\sigma_{i+1}^{k-j+1})-(\sigma_{i-1}^{k-j}+4\sigma_i^{k-j}+\sigma_{i+1}^{k-j})\Big].\end{aligned}$$

System (13) consists of $(M+1)$ linear equations in $(M+3)$ unknowns

$$(\sigma_{-1}^{k+1}, \sigma_0^{k+1}, \sigma_1^{k+1}, \ldots, \sigma_M^{k+1}, \sigma_{M+1}^{k+1}).$$

To obtain a unique solution to the resulting system two additional constraints are required. These are obtained by imposing boundary conditions (3). Eliminating σ_{-1}, and σ_{M+1} the system gets reduced to a matrix system of dimension $(M+1) \times (M+1)$ as follows

$$\Gamma \mathcal{X} = \Upsilon, \tag{14}$$

where

$$\Gamma = \begin{pmatrix} \mu_2 - 4\mu_1 & \mu_3 - \mu_1 & 0 & \ldots & \ldots & 0 & 0 & 0 \\ \mu_1 & \mu_2 & \mu_3 & \ldots & \ldots & 0 & 0 & 0 \\ \vdots & \vdots & \vdots & \vdots & \vdots & \vdots & \vdots & \vdots \\ \vdots & \vdots & \vdots & \vdots & \vdots & \vdots & \vdots & \vdots \\ 0 & 0 & 0 & \ldots & \ldots & \mu_1 & \mu_2 & \mu_3 \\ 0 & 0 & 0 & \ldots & \ldots & 0 & \mu_1 - \mu_3 & \mu_2 - 4\mu_3 \end{pmatrix},$$

$$\mathcal{X} = \begin{pmatrix} \sigma_0^{k+1} \\ \sigma_1^{k+1} \\ \vdots \\ \vdots \\ \sigma_{M-1}^{k+1} \\ \sigma_M^{k+1} \end{pmatrix}, \qquad \Upsilon = \begin{pmatrix} \mathcal{A}(x_0, t_{k+1}) - \mu_1 r_2(t_{k+1}) \\ \mathcal{A}(x_1, t_{k+1}) \\ \vdots \\ \vdots \\ \mathcal{A}(x_{M-1}, t_{k+1}) \\ \mathcal{A}(x_M, t_{k+1}) - \mu_3 r_3(t_{k+1}) \end{pmatrix}.$$

System (14) is a tridiagonal system that can be solved by Thomas algorithm [19]. Finally, we can obtain

$$\varphi^*(x_i, t_k) = \sigma_{i-1}^k + 4\sigma_i^k + \sigma_{i+1}^k, \qquad i = 0, 1, \ldots, M, \qquad k = 1, 2, \ldots$$

3.4. **The initial vector.** At each time step, the approximate solution $\varphi(x,t)$ is obtained iteratively, provided that the initial conditions are well-defined.
From the initial condition

$$\varphi^*(x_i, 0) = r_1(x_i), \qquad i = 0, 1, \ldots, M,$$

we get $(M+1)$ equations in $(M+3)$ unknowns $(\sigma_{-1}^0, \sigma_0^0, \sigma_1^0, \ldots, \sigma_M^0, \sigma_{M+1}^0)$. The two unknowns σ_{-1}^0 and σ_{M+1}^0 can be obtained from the relation $\varphi_x^*(x_0, 0) = r_1'(x_0)$ and $\varphi_x^*(x_M, 0) = r_1'(x_M)$ at the knots. It leads to a system of $(M+1)$ equations in $(M+1)$

unknowns as follows

$$\begin{pmatrix} 4 & 2 & 0 & 0 & \dots & \dots & 0 & 0 & 0 & 0 \\ 1 & 4 & 1 & 0 & \dots & \dots & 0 & 0 & 0 & 0 \\ \vdots & \vdots & \vdots & \vdots & \vdots & \vdots & \vdots & \vdots & \vdots & \vdots \\ \vdots & \vdots & \vdots & \vdots & \vdots & \vdots & \vdots & \vdots & \vdots & \vdots \\ 0 & 0 & 0 & 0 & \dots & \dots & 0 & 1 & 4 & 1 \\ 0 & 0 & 0 & 0 & \dots & \dots & 0 & 0 & 2 & 4 \end{pmatrix} \begin{pmatrix} \sigma_0^0 \\ \sigma_1^0 \\ \vdots \\ \vdots \\ \sigma_{M-1}^0 \\ \sigma_M^0 \end{pmatrix} = \begin{pmatrix} r_1(x_0) + \frac{h_x}{3} r_1'(x_0) \\ r_1(x_1) \\ \vdots \\ \vdots \\ r_1(x_{M-1}) \\ r_1(x_M) - \frac{h_x}{3} r_1'(x_M) \end{pmatrix},$$

which can be solved by Thomas algorithm.

4. Convergence analysis

Theorem 4.1. *The collocation approximation $\varphi_k^*(x)$ for the solution $\varphi_k(x)$ of the problem* (1)–(3) *satisfy the following error estimate*

$$\left\| \varphi_k - \varphi_k^* \right\|_\infty \leq \zeta h_x^4,$$

for sufficiently small h_x (i.e. for sufficiently large M) where ζ is a positive constant.

Proof. Let $\varphi_k(x)$ is the exact solution of the problem (1)–(3). Also, we set

$$\varphi_k^*(x) = \sum_{i=-1}^{M+1} \sigma_i^k B_i(x),$$

to be B-spline collocation approximation to $\varphi_k(x)$. Due to round off errors in computations, we assume that $\widetilde{\varphi^*}_k(x)$ is the computed spline for $\varphi_k^*(x)$ so that

$$\widetilde{\varphi^*}_k(x) = \sum_{i=-1}^{M+1} \widetilde{\sigma}_i^n B_i(x).$$

To estimate the error $||\varphi_k(x) - \varphi_k^*(x)||_\infty$, it is needed to estimate the errors

$$||\varphi_k(x) - \widetilde{\varphi^*}_k(x)||_\infty \text{ and } ||\widetilde{\varphi^*}_k(x) - \varphi_k^*(x)||_\infty,$$

separately. Following (14) for $\widetilde{\varphi^*}_k$ we have

$$\Gamma \widetilde{\mathcal{X}} = \widetilde{\Upsilon}, \tag{15}$$

where

$$\widetilde{\mathcal{X}} = \left[\widetilde{\sigma}_0^{k+1}, \widetilde{\sigma}_1^{k+1}, \dots, \widetilde{\sigma}_{M-1}^{k+1}\ \widetilde{\sigma}_M^{k+1}\right]^T,$$

$$\widetilde{\Upsilon} = \left[\widetilde{\mathcal{A}}(x_0, t_{k+1}) - \mu_1 r_2(t_{k+1}), \widetilde{\mathcal{A}}(x_1, t_{k+1}), \dots, \widetilde{\mathcal{A}}(x_{M-1}, t_{k+1}), \widetilde{\mathcal{A}}(x_M, t_{k+1}) - \mu_3 r_3(t_{k+1})\right]^T.$$

By subtracting (14) and (15) we have

$$\Gamma\Big(\mathcal{X} - \widetilde{\mathcal{X}}\Big) = \Big(\Upsilon - \widetilde{\Upsilon}\Big). \tag{16}$$

On the other hand

$$\Upsilon - \widetilde{\Upsilon} = \begin{bmatrix} \mathcal{A}(x_0, t_{k+1}) - \widetilde{\mathcal{A}}(x_0, t_{k+1}) \\ \mathcal{A}(x_1, t_{k+1}) - \widetilde{\mathcal{A}}(x_1, t_{k+1}) \\ \vdots \\ \mathcal{A}(x_{M-1}, t_{k+1}) - \widetilde{\mathcal{A}}(x_{M-1}, t_{k+1}) \\ \mathcal{A}(x_M, t_{k+1}) - \widetilde{\mathcal{A}}(x_M, t_{k+1}) \end{bmatrix} \tag{17}$$

such that for every $0 \leq i \leq M$,

$$\mathcal{A}(x_i, t_{k+1}) = \mathcal{G}(x_i, t_{k+1}) + \delta\varphi^*(x_i, t_k) - \alpha_2\gamma^* \sum_{j=1}^{k} \omega_{j,i}^{k+1} \Big[\varphi^*(x_i, t_{k-j+1}) - \varphi^*(x_i, t_{k-j})\Big],$$

$$\widetilde{\mathcal{A}}(x_i, t_{k+1}) = \mathcal{G}(x_i, t_{k+1}) + \delta\widetilde{\varphi^*}(x_i, t_k) - \alpha_2\gamma^* \sum_{j=1}^{k} \omega_{j,i}^{k+1} \Big[\widetilde{\varphi^*}(x_i, t_{k-j+1}) - \widetilde{\varphi^*}(x_i, t_{k-j})\Big].$$

So,

$$\begin{aligned} \Big|\mathcal{A}(x_i, t_{k+1}) - \widetilde{\mathcal{A}}(x_i, t_{k+1})\Big| &\leq \delta\Big|\varphi^*(x_i, t_k) - \widetilde{\varphi^*}(x_i, t_k)\Big| \\ &+ \alpha_2\gamma^* \sum_{j=1}^{k} \omega_{j,i}^{k+1} \Bigg[\Big|\varphi^*(x_i, t_{k-j+1}) - \widetilde{\varphi^*}(x_i, t_{k-j+1})\Big| + \Big|\varphi^*(x_i, t_{k-j}) - \widetilde{\varphi^*}(x_i, t_{k-j})\Big|\Bigg]. \end{aligned}$$

From Hall and Meyer error estimate ([8]), we get

$$\Big\|D^r(\varphi^*(x, t_k) - \widetilde{\varphi^*}(x, t_k))\Big\|_\infty \leq \varepsilon_r \Big\|\frac{d^4\varphi^*(x, t_k)}{dx^4}\Big\|_\infty h_x^{4-r}, \qquad r = 0, 1, 2, 3. \tag{18}$$

Therefore,

$$\begin{aligned} \Big|\mathcal{A}(x_i, t_{k+1}) - \widetilde{\mathcal{A}}(x_i, t_{k+1})\Big| &\leq \delta\varepsilon_0 \Big\|\frac{d^4\varphi^*(x, t_k)}{dx^4}\Big\|_\infty h_x^4 \\ &+ \alpha_2\gamma^* \sum_{j=1}^{k} \omega_{j,i}^{k+1} \Bigg[\varepsilon_0 \Big\|\frac{d^4\varphi^*(x, t_{k-j+1})}{dx^4}\Big\|_\infty h_x^4 + \varepsilon_0 \Big\|\frac{d^4\varphi^*(x, t_{k-j})}{dx^4}\Big\|_\infty h_x^4\Bigg], \end{aligned} \tag{19}$$

and hence,

$$\Big|\mathcal{A}(x_i, t_{k+1}) - \widetilde{\mathcal{A}}(x_i, t_{k+1})\Big| \leq h_x^4 \Big(\delta\varepsilon_0 L + 2\alpha_2\gamma^*\varepsilon_0 L((k+1)^{1-\lambda_i^{k+1}} - 1)\Big). \tag{20}$$

From (20), is deduced that

$$||\Upsilon - \widetilde{\Upsilon}||_\infty \leq \varsigma h_x^4, \tag{21}$$

where

$$\varsigma = \delta\varepsilon_0 L + 2\alpha_2\gamma^*\varepsilon_0 L((k+1)^{1-\lambda_i^{k+1}} - 1).$$

Also, from (16), we have

$$\mathcal{X} - \widetilde{\mathcal{X}} = \Gamma^{-1}(\Upsilon - \widetilde{\Upsilon}).$$

Taking the infinity norm, then using (21), one can deduce that

$$\Big\|\mathcal{X} - \widetilde{\mathcal{X}}\Big\|_\infty = \Big\|\Gamma^{-1}\Big\|_\infty \Big\|\Upsilon - \widetilde{\Upsilon}\Big\|_\infty \leq \varsigma h_x^4 \Big\|\Gamma^{-1}\Big\|_\infty = \widetilde{\varsigma} h_x^4,$$

where $\widetilde{\varsigma} = \varsigma \left\| \Gamma^{-1} \right\|_\infty$. Now, we compute $\left\| \varphi_k - \varphi_k^* \right\|_\infty$ as the following

$$\left\| \varphi_k - \varphi_k^* \right\|_\infty = \left\| \varphi_k - \widetilde{\varphi^*}_k \right\|_\infty + \left\| \widetilde{\varphi^*}_k - \varphi_k^* \right\|_\infty,$$

such that

$$\varphi_k^*(x) - \widetilde{\varphi^*}_k(x) = \sum_{i=-1}^{M+1} (\sigma_i^k - \widetilde{\sigma}_i^k) B_i(x).$$

So,

$$\left| \varphi_k^*(x_m) - \widetilde{\varphi^*}_k(x_m) \right| \leq \max_{-1 \leq i \leq M+1} \left\{ |\sigma_i^k - \widetilde{\sigma}_i^k| \right\} \sum_{i=-1}^{M+1} |B_i(x_m)|, \qquad 0 \leq m \leq M.$$

By using the values of $B_i(x_m)$'s given in Section 2, we have $\sum_{i=-1}^{M+1} |B_i(x_m)| \leq 10$, $0 \leq m \leq N$ (see, [9]); Therefore,

$$\left\| \varphi_k^* - \widetilde{\varphi^*}_k \right\|_\infty \leq 10 \widetilde{\varsigma} h_x^4. \tag{22}$$

So, according to equations (18) and (22), we obtain

$$\begin{aligned} \left\| \varphi_k - \varphi_k^* \right\|_\infty &\leq \varepsilon_0 L h_x^4 + 10 \widetilde{\varsigma} h_x^4 \\ &= h_x^4 \Big(\varepsilon_0 L + 10 \widetilde{\varsigma} \Big). \end{aligned}$$

Setting $\zeta = \varepsilon_0 L + 10\widetilde{\varsigma}$, we have

$$\left\| \varphi_k - \varphi_k^* \right\|_\infty \leq \zeta h_x^4.$$

□

As a result of Theorem 4.1 we have the following theorem.

Theorem 4.2. *Suppose that $\varphi^*(x, t_k)$ be the collocation approximation of the exact solution $\varphi(x, t_k)$. Then the error estimate of the totally discrete scheme is calculated as:*

$$\left\| \varphi_k - \varphi_k^* \right\|_\infty \leq \kappa (h_t^{2-\lambda(x,t_{k+1})} + h_x^4),$$

where κ is some finite constant.

Remark 4.1. *According to Theorem 4.2, the order of convergence of our method is theoretically $\mathcal{O}(h_t^{2-\lambda(x,t)} + h_x^4)$, where $\lambda(x,t)$ is the variable fractional order. However, in practical computations and in line with common practice, we report the dominant error order of the time discretization scheme. For variable-order problems, this is typically $\mathcal{O}(h_t^2)$ when $\lambda(x,t)$ remains sufficiently small or smooth over the domain.*

5. Numerical Computations and Results

This section presents the numerical computations of the time-variable fractional order MIM-ADM (1) under the initial and boundary conditions (2) and (3). To evaluate the performance of the proposed method, two numerical examples are provided with error norms L_2 and L_∞ for $x \in [0,1]$ and $t \in [0, t_{\text{final}}]$, defined as follows:

$$L_2 = \sqrt{h_x \sum_{i=1}^{M} (\varphi_{\text{exact}}(x_i,t) - \varphi_{\text{approx}}(x_i,t))^2}, \qquad \text{where} \qquad h_x = \frac{1}{M},$$

$$L_\infty = \|\varphi_{\text{exact}}(x,t) - \varphi_{\text{approx}}(x,t)\|_\infty = \max |\varphi_{\text{exact}}(x,t) - \varphi_{\text{approx}}(x,t)|\,,$$

In the following numerical examples, we take $\alpha_1 = \alpha_2 = \theta_1 = \theta_2 = 1$. Therefore, we have:

$$\frac{\partial \varphi(x,t)}{\partial t} + D_t^{\lambda(x,t)} \varphi(x,t) = -\frac{\partial \varphi(x,t)}{\partial x} + \frac{\partial^2 \varphi(x,t)}{\partial x^2} + \mathcal{G}(x,t), \quad (x,t) \in [0,1] \times [0,1]. \quad (23)$$

These examples were solved by Zhang et al. using the implicit Euler approximation [21]. MATLAB (R2015b) was used for the graphical analysis and numerical computations in this paper.

Remark 5.1. *The convergence rate of $\varphi(x,t)$, with time step length h_t of the time discretization (denoted by P_1) and with space step length h_x of the space discretization (denoted by P_2) can be calculated by the following formulas;*

$$P_1 = \frac{\log_{10}\Big((L_\infty)_{h_t^1}/(L_\infty)_{h_t^2}\Big)}{\log_{10}(h_t^1/h_t^2)}, \qquad P_2 = \frac{\log_{10}\Big((L_\infty)_{h_x^1}/(L_\infty)_{h_x^2}\Big)}{\log_{10}(h_x^1/h_x^2)}. \quad (24)$$

To evaluate the convergence rate of the proposed method in the time and space directions, we respectively consider $h_t = h_x = 0.1, 0.05, 0.025$.
In Tables 2, 3, and 5, absolute errors for different spatial points are presented to illustrate the accuracy of the proposed method. The explicit convergence rates, computed using the L_∞ norm as described in formula (24), are summarized in Tables 6 and 7 for the corresponding examples. According to Remark 4.1, the observed convergence rates in Tables 6 and 7 are in agreement with the practical order discussed therein.

5.1. **Test Problems.**

Example 5.1. *In this example, we consider the time-variable fractional order MIM-ADM* (23)*, where*

$$\begin{aligned}
\lambda(x,t) &= 1 - 0.5e^{-xt}, \\
\mathcal{G}(x,t) &= 10x^2(1-x)^2 + \frac{10x^2(1-x)^2 t^{1-\lambda(x,t)}}{\Gamma(2-\lambda(x,t))} + 10(t+1)(2x - 6x^2 + 4x^3) \\
&\quad - 10(t+1)(2 - 12x + 12x^2).
\end{aligned}$$

The exact solution of this example is $\varphi(x,t) = 10(t+1)x^2(1-x)^2$ and the initial and boundary conditions are derived accordingly.
In Table 2, we compare our method with the proposed method given in [21] *for the absolute errors between exact and approximate solutions at the final time $t = 1$. In Figure 1, we show the L_2 and L_∞ errors for $\varphi(x,t)$ at different space levels. The comparison between the exact and approximate solution $\varphi(x,t)$ at different time levels are given in Figure 2.*

TABLE 2. The comparison among the exact and approximate solutions for $\varphi(x,1)$ in Example 5.1.

x	φ_{exact}	Method of [21]		Proposed Method	
		φ_{approx}	$\lvert\varphi_{\text{exact}}-\varphi_{\text{approx}}\rvert$	φ_{approx}	$\lvert\varphi_{\text{exact}}-\varphi_{\text{approx}}\rvert$
0.1	0.1620	0.1618	$1.5629e-04$	0.1619	$1.3895e-04$
0.2	0.5120	0.5106	$1.4007e-03$	0.5117	$2.5251e-04$
0.3	0.8820	0.8790	$2.9752e-03$	0.8817	$3.3973e-04$
0.4	1.1520	1.1477	$4.2977e-03$	1.1516	$3.9911e-04$
0.5	1.2500	1.2450	$4.9722e-03$	1.2496	$4.2858e-04$
0.6	1.1520	1.1472	$4.8034e-03$	1.1516	$4.2536e-04$
0.7	0.8820	0.8782	$3.8153e-03$	0.8816	$3.8588e-04$
0.8	0.5120	0.5097	$2.2747e-03$	0.5117	$3.0570e-04$
0.9	0.1620	0.1613	$7.2075e-04$	0.1618	$1.7930e-04$
Execution time (second)				329.831447	

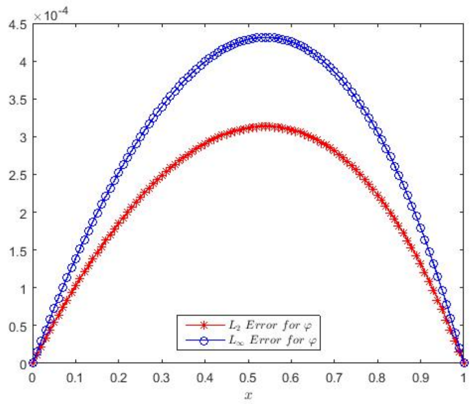

FIGURE 1. The L_2 and L_∞ errors of Example 5.1 at different space levels.

Example 5.2. *In this example, we consider the time-variable fractional order MIM-ADM* (23)*, where*

$$\lambda(x,t) = 0.8 + 0.005\cos(xt)\sin(x),$$

$$\mathcal{G}(x,t) = 5x(1-x) + \frac{5x(1-x)t^{1-\lambda(x,t)}}{\Gamma(2-\lambda(x,t))} + 5(t+1)(1-2x) + 10(t+1).$$

The exact solution of this example is $\varphi(x,t) = 5(t+1)x(1-x)$ and the initial and boundary conditions are derived accordingly.
In Table 3, we compare the exact and approximate solutions at the final time $t = 1$. In Figure 3, we show the L_2 and L_∞ errors for $\varphi(x,t)$ at different space levels. The comparison between the exact and approximate solution $\varphi(x,t)$ at different time levels are given in Figure 4.

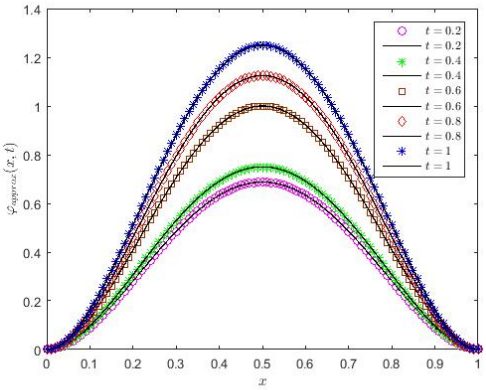

FIGURE 2. The comparison between the exact solution (shown by continuous lines) and approximate solution (using the proposed method) of $\varphi(x,t)$ at different time levels for Example 5.1

Furthermore, the comparison L_∞ *error in Examples 5.1 and 5.2 for different values of* h_x *and* h_t*, is provided in Table 4.*

TABLE 3. The comparison among the exact and approximate solutions for $\varphi(x,1)$ in Example 5.2.

x	φ_{exact}	φ_{approx}	$\lvert\varphi_{\text{exact}}-\varphi_{\text{approx}}\rvert$
0.1	0.900000	0.900000	$1.110223e-16$
0.2	1.600000	1.600000	$2.220446e-16$
0.3	2.100000	2.100000	0
0.4	2.400000	2.400000	0
0.5	2.500000	2.500000	$4.440892e-16$
0.6	2.400000	2.400000	0
0.7	2.100000	2.100000	0
0.8	1.600000	1.600000	0
0.9	0.900000	0.900000	$1.110223e-16$
Execution time (second)		335.068427	

Example 5.3. *In this example, we consider the time-variable fractional order MIM-ADM* (23)*, where*

$$\lambda(x,t) = 1 - 0.5e^{-xt},$$

$$\mathcal{G}(x,t) = 5(1+\pi^2(t+1))\sin(\pi x) + \frac{5\sin(\pi x)t^{1-\lambda(x,t)}}{\Gamma(2-\lambda(x,t))} + 5\pi(t+1)\cos(\pi x).$$

The exact solution of this example is $\varphi(x,t) = 5(t+1)\sin(\pi x)$ *and the initial and boundary conditions are derived accordingly.*

In Table 5, we compare the exact and approximate solutions at the final time $t = 1$*.*

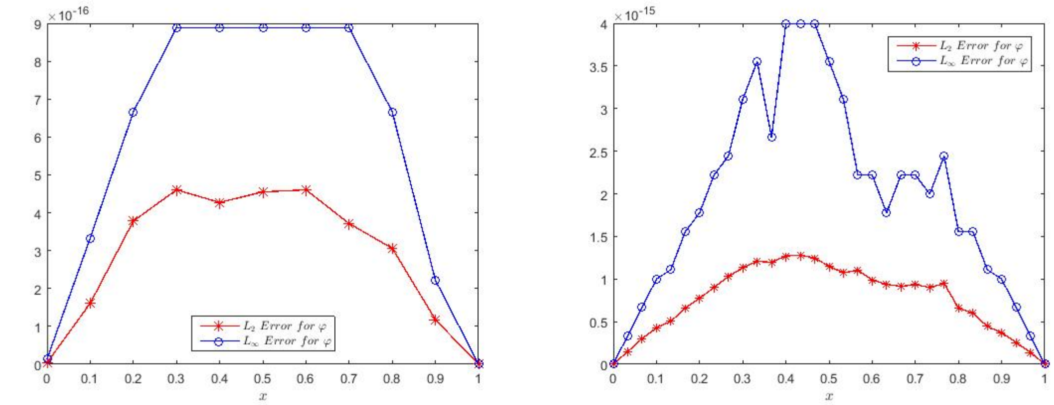

FIGURE 3. The L_2 and L_∞ errors of Example 5.2 at different space levels.

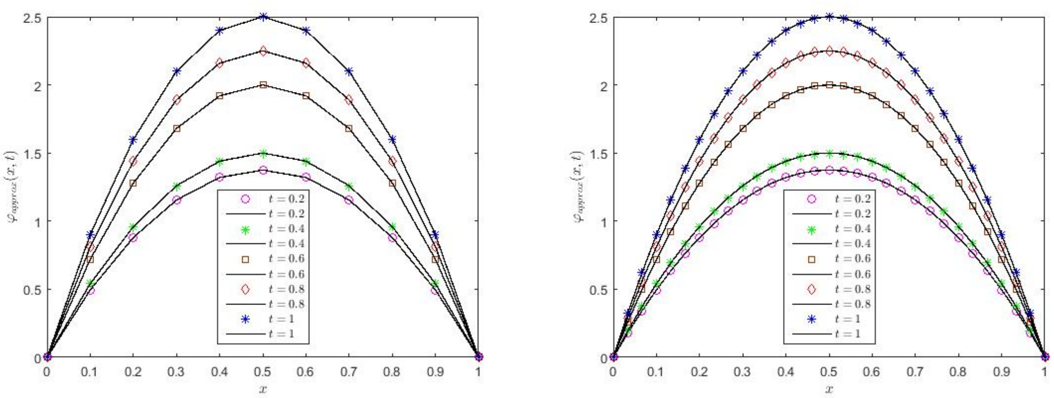

FIGURE 4. The comparison between the exact solution (shown by continuous lines) and approximate solution (using the proposed method) of $\varphi(x, t)$ at different time levels for Example 5.2

TABLE 4. The comparison L_∞ error in Examples 5.1 and 5.2 for different values of h_x and h_t.

$h_x = h_t$	Example 5.1		Example 5.2	
	Method of [21]	Proposed Method	Method of [21]	Proposed Method
$1/50$	$9.4391e-03$	$1.7291e-03$	$2.1562e-02$	$3.3307e-15$
$1/100$	$5.0134e-03$	$4.3234e-04$	$1.0825e-02$	$9.7700e-15$

In Figure 5, we show the L_2 and L_∞ errors for $\varphi(x, t)$ at different space levels. The comparison between the exact and approximate solution $\varphi(x, t)$ at different time levels are given in Figure 6.

6. CONCLUSION

In this paper, we have developed a hybrid numerical method that integrates the cubic B-spline collocation method and the implicit Euler approximation to solve the MIM-ADM.

Table 5. The comparison among the exact and approximate solutions for $\varphi(x,1)$ in Example 5.3.

x	φ_{exact}	φ_{approx}	$\lvert\varphi_{\text{exact}} - \varphi_{\text{approx}}\rvert$
0.1	3.090170	3.089982	$1.879619e-04$
0.2	5.877853	5.877480	$3.726123e-04$
0.3	8.090170	8.089637	$5.327227e-04$
0.4	9.510565	9.509916	$6.492514e-04$
0.5	10.000000	9.999293	$7.071503e-04$
0.6	9.510565	9.509868	$6.967765e-04$
0.7	8.090170	8.089555	$6.147649e-04$
0.8	5.877853	5.877388	$4.642728e-04$
0.9	3.090170	3.089915	$2.545684e-04$
Execution time (second)		328.881762	

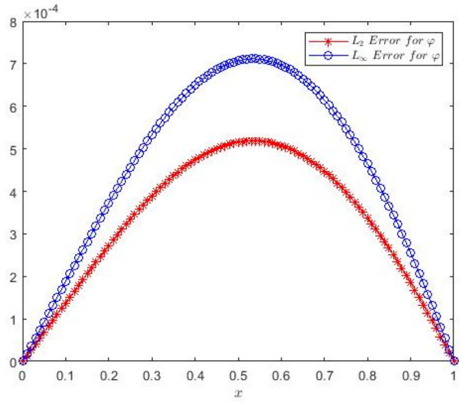

Figure 5. The L_2 and L_∞ errors of Example 5.3 at different space levels.

The adoption of the Coimbra variable-order fractional derivative has proven effective in capturing the complex behavior of transport processes in porous media, which traditional integer-order models fail to accurately describe. The proposed method leverages the flexibility and high accuracy of cubic B-splines for spatial discretization, alongside the robustness of the implicit Euler approximation for time fractional derivatives. This combination offers a powerful framework for modeling and solving the MIM-ADM with VO derivatives. Additionally, we have established that the method achieves a theoretical convergence order of $\mathcal{O}(h_t^{2-\lambda(x,t)} + h_x^4)$, where $\lambda(x,t)$ is the variable fractional order. In practical computations, when $\lambda(x,t)$ remains sufficiently small or smooth over the domain, the dominant temporal error order is typically $\mathcal{O}(h_t^2)$, as confirmed by our numerical experiments. Numerical experiments have demonstrated the effectiveness and accuracy of the proposed method. Furthermore, the plotted graphs confirmed the reliability of the proposed method.

Future work will focus on further refining the numerical method to improve its efficiency

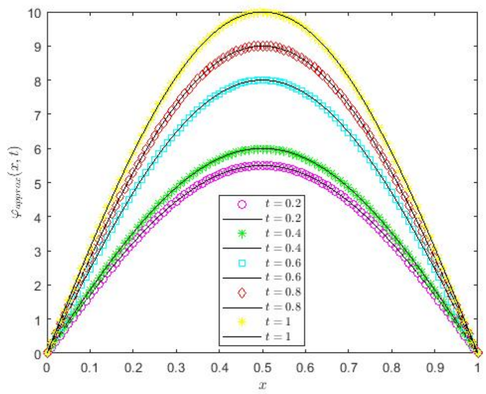

FIGURE 6. The comparison between the exact solution (shown by continuous lines) and approximate solution (using the proposed method) of $\varphi(x,t)$ at different time levels for Example 5.3

TABLE 6. The convergence rate in time direction for $\varphi(x,t)$.

	h_t	L_∞	Error rate P_1
Example 5.1	0.1	$4.2858e-04$	-
	0.05	$1.2315e-04$	1.7991
	0.025	$3.3142e-05$	1.8937
Example 5.2	0.1	$4.4409e-16$	-
	0.05	$1.1938e-16$	1.8953
	0.025	$3.1072e-17$	1.9419
Example 5.3	0.1	$7.071503e-04$	-
	0.05	$1.796549e-04$	1.9768
	0.025	$4.494691e-05$	1.9989

and extend its applicability to a broader range of complex transport phenomena. Additionally, the development of more sophisticated variable-order fractional models and their integration with advanced numerical techniques will be explored to continue advancing the field of fractional calculus and its applications in modeling complex systems.

References

[1] Amin, M., Abbas, M., Iqbal, M. K. and Baleanu, D., (2020), Numerical treatment of time-fractional Klein–Gordon equation using redefined extended cubic B-spline functions, Frontiers in Physics, 8, 288.

[2] Baleanu, D., Machado, J. A. T. and Luo, A. C., (2011), Fractional dynamics and control, Springer Science & Business Media.

[3] Coimbra, C. F., (2003), Mechanics with variable-order differential operators, Annalen der Physik, 515 (11-12), pp. 692–703.

[4] Foadian, S., Pourgholi, R. and Hashem Tabasi, S., (2018), Cubic B-spline method for the solution of an inverse parabolic system, Applicable Analysis, 97 (3), pp. 438–465.

TABLE 7. The convergence rate in space direction for $\varphi(x,t)$.

	h_x	L_∞	Error rate P_2
Example 5.1	0.1	$4.2858e-04$	-
	0.05	$3.0565e-05$	3.8096
	0.025	$2.0434e-06$	3.9028
Example 5.2	0.1	$4.4409e-16$	-
	0.05	$2.9744e-17$	3.9002
	0.025	$1.9920e-18$	3.9003
Example 5.3	0.1	$7.071503e-04$	-
	0.05	$4.560789e-05$	3.9547
	0.025	$2.919987e-06$	3.9652

[5] Golbabai, A., Nikan, O. and Nikazad, T., (2019), Numerical investigation of the time fractional mobile-immobile advection-dispersion model arising from solute transport in porous media, International Journal of Applied and Computational Mathematics, 5, pp. 1–22.

[6] Gupta, R. and Kumar, S., (2023), Chebyshev spectral method for the variable-order fractional mobile–immobile advection–dispersion equation arising from solute transport in heterogeneous media, Journal of Engineering Mathematics, 142 (1), 1.

[7] Gupta, R. and Kumar, S., (2024), Space-time pseudospectral method for the variable-order space-time fractional diffusion equation, Mathematical Sciences, 18 (3), pp. 419–436.

[8] Hall, C. A. and Meyer, W. W., (1976), Optimal error bounds for cubic spline interpolation, Journal of Approximation Theory, 16 (2), pp. 105–122.

[9] Kadalbajoo, M. K., Gupta, V. and Awasthi, A., (2008), A uniformly convergent B-spline collocation method on a nonuniform mesh for singularly perturbed one-dimensional time-dependent linear convection–diffusion problem, Journal of Computational and Applied Mathematics, 220 (1-2), pp. 271–289.

[10] Kamran, Khan, S., Alhazmi, S. E., Alotaibi, F. M., Ferrara, M. and Ahmadian, A., (2022), On the numerical approximation of mobile-immobile advection-dispersion model of fractional order arising from solute transport in porous media, Fractal and Fractional, 6 (8), 445.

[11] Kharisa, A., Maryani, S. and Nurhayati, N., (2022), Solution of the second order of the linear hyperbolic equation using cubic B-spline collocation numerical method, JTAM (Jurnal Teori dan Aplikasi Matematika), 6 (2), pp. 438–447.

[12] Mittal, R. and Tripathi, A., (2015), Numerical solutions of generalized burgers–fisher and generalized burgers–huxley equations using collocation of cubic B-splines, International Journal of Computer Mathematics, 92 (5), pp. 1053–1077.

[13] Patnaik, S., Hollkamp, J. P. and Semperlotti, F., (2020), Applications of variable-order fractional operators: a review, Proceedings of the Royal Society A, 476 (2234), 20190498.

[14] Podlubny, I., (1998), Fractional differential equations: an introduction to fractional derivatives, fractional differential equations, to methods of their solution and some of their applications, Elsevier.

[15] Prenter, P. M., et al., (2008), Splines and variational methods, Courier Corporation.

[16] Ray, S. S., (2022), A novel wavelets operational matrix method for the time variable-order fractional mobile–immobile advection–dispersion model, Engineering with Computers, 38 (Suppl 4), pp. 2629–2650.

[17] Shafiq, M., Abbas, M., Abdullah, F. A., Majeed, A., Abdeljawad, T. and Alqudah, M. A., (2022), Numerical solutions of time fractional burgers' equation involving atangana–baleanu derivative via cubic b-spline functions, Results in Physics, 34, 105244.

[18] Sun, H., Chang, A., Zhang, Y. and Chen, W., (2019), A review on variable-order fractional differential equations: mathematical foundations, physical models, numerical methods and applications, Fractional Calculus and Applied Analysis, 22 (1), pp. 27–59.
[19] Von Rosenberg, D. U., (1969), Methods for the numerical solution of partial differential equations, American Elsevier Pub. Co.
[20] Wei, L. and Yang, Y., (2021), Optimal order finite difference/local discontinuous Galerkin method for variable-order time-fractional diffusion equation, Journal of Computational and Applied Mathematics, 383, 113129.
[21] Zhang, H., Liu, F., Phanikumar, M. S. and Meerschaert, M. M., (2013), A novel numerical method for the time variable fractional order mobile–immobile advection–dispersion model, Computers & Mathematics with Applications, 66 (5), pp. 693–701.
[22] Zhang, X., Feng, Y., Luo, Z. and Liu, J., (2025), A spatial sixth-order numerical scheme for solving fractional partial differential equation, Applied Mathematics Letters, 159, 109265.

Saedeh Foadian received her B.Sc. degree in applied mathematics (2009), her M.Sc. degree in harmonic analysis (2012), and her Ph.D. degree in 2018 in Applied Mathematics at Damghan University, Iran. Her area of research is the numerical solution of linear and nonlinear partial differential equations.

Reza Pourgholi received his M.Sc. degree in 2001 and a Ph.D. degree in 2007 in Applied Mathematics from IUST, Tehran, Iran. He is now a full professor at Damghan University. His area of research is the numerical solution of inverse problems in partial differential equations.